research papers

JOURNAL OF SYNCHROTRON RADIATION

ISSN 1600-5775

Received 15 November 2014
Accepted 16 February 2015

Edited by G. E. Ice, Oak Ridge National Laboratory, USA

Keywords: direct-write X-ray lithography; X-ray writer; Fresnel zone plate; proximity effect; backscattered electrons.

Direct-write X-ray lithography using a hard X-ray Fresnel zone plate

Su Yong Lee,[a] Do Young Noh,[a]* Hae Cheol Lee,[b] Chung-Jong Yu,[b] Yeukuang Hwu[c] and Hyon Chol Kang[d]*

[a]Department of Physics and Photon Science and School of Materials Science and Engineering, Gwangju Institute of Science and Technology, 123 Cheomdangwagi-ro, Buk-gu, Gwangju 500-712, South Korea, [b]Pohang Accelerator Laboratory, POSTECH, 80 Jigokro-127-beongil, Nam-gu, Pohang, Gyeongbuk 790-834, South Korea, [c]Institute of Physics, Academia Sinica, Taipei 11529, Taiwan, and [d]Department of Materials Science and Engineering, Chosun University, 309 Pilmun-daero, Dong-gu, Gwangju 501-759, South Korea. *Correspondence e-mail: dynoh@gist.ac.kr, kanghc@chosun.ac.kr

Results are reported of direct-write X-ray lithography using a hard X-ray beam focused by a Fresnel zone plate with an outermost zone width of 40 nm. An X-ray beam at 7.5 keV focused to a nano-spot was employed to write arbitrary patterns on a photoresist thin film with a resolution better than 25 nm. The resulting pattern dimension depended significantly on the kind of underlying substrate, which was attributed to the lateral spread of electrons generated during X-ray irradiation. The proximity effect originated from the diffuse scattering near the focus and electron blur was also observed, which led to an increase in pattern dimension. Since focusing hard X-rays to below a 10 nm spot is currently available, the direct-write hard X-ray lithography developed in this work has the potential to be a promising future lithographic method.

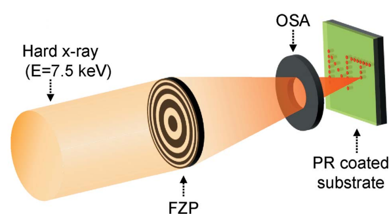

© 2015 International Union of Crystallography

1. Introduction

Lithography techniques have been critical for fabricating various sub-micrometer-scale devices in the fields of electronics, medical diagnostics and mechanical components. Recent progress in advanced lithography systems have realised high-resolution patterns with dimensions below a few nanometers, and there is on-going research to explore the fundamental limits of lithography on the atomic sub-nanometer scale (Chou *et al.*, 1997; Macintyre & Thoms, 2011; Winston *et al.*, 2011). Unlike mask-based lithography, whose resolution is critically limited by the dimensions of the masks (Suzuki & Smith, 2007), 'direct-write lithography' is free of masks and capable of creating arbitrary patterns. In this maskless lithography technique, typically a light or particle beam is focused to a small spot size by means of a suitable focusing device, which illuminates photoresist (PR). Consequently, the focusing capability is a key factor in determining the resolution of a direct-write process, although the sensitivity of PR materials and parasitic exposure must also be considered carefully. Up to now, among various direct-write processes such as electron-beam lithography, ion beam lithography (Winston *et al.*, 2011) and focused laser lithography (Gan *et al.*, 2013), direct-write electron-beam lithography (e-beam writers) has been widely used for practical purposes, and patterns as small as 5 nm have been achieved with great success (Macintyre & Thoms, 2011).

Recently, there has been a considerable amount of effort devoted to developing direct-write X-ray lithography (X-ray writers) using synchrotron light sources (Caster *et al.*, 2010; Leontowich & Hitchcock, 2011; Leontowich *et al.*, 2013). The concept of X-ray writers, *i.e.* maskless lithography, is similar to

that of an e-beam writer, but offers a unique way to overcome limited scan area and vacuum requirements inherent to e-beam writers. Particular interest lies in the fact that X-ray writers are free from charging which limits the application of e-beam writers to insulating substrates (Satyalakshmi *et al.*, 2000). The short wavelength of X-rays (0.1–1 nm) is also highly desirable in terms of the patterning resolution. Nevertheless, the development of X-ray writers has been greatly hampered by the inherent difficulties in manufacturing suitably high-resolution focusing optics due to the penetrating nature of X-rays and their weak interaction with materials (Bergemann *et al.*, 2003; Schroer & Lengeler, 2005; Kang *et al.*, 2006). Recent advancements in X-ray focusing optics capable of producing nano-sized spots (Schroer *et al.*, 2005; Kang *et al.*, 2006; Mimura *et al.*, 2009; Chen *et al.*, 2011; Huang *et al.*, 2013; Keskinbora *et al.*, 2014), however, have greatly increased the performance of X-ray writers. For example, Leontowich *et al.* (2013) have demonstrated an X-ray writer with a resolution of 25 nm in the soft X-ray regime ($E \leq 1$ keV), in which they used a Fresnel zone plate (FZP) as the focusing optic. This FZP is a diffractive optic system composed of alternating concentric opaque and transparent zones that satisfy the zone plate law. Two critical issues related to the FZPs are reducing the size of focus to the fundamental limit and obtaining a high focusing efficiency (Kirz, 1974; Wu *et al.*, 2012). Note that the size of focus is defined by $R = 1.22\Delta r_n$, where Δr_n is the outermost zone width. Up to now, FZPs with Δr_n = 12 nm have exhibited the best resolution (Chao *et al.*, 2012).

The focusing efficiency is mainly determined by the positioning accuracy and depth of zones (z) along the optical axis. Hard X-rays of photon energy above 7 keV with much shorter wavelength than soft X-rays are more favorable in obtaining smaller focal-spots considering the simple dependence of the diffraction limits on wavelength. However, significant technological challenges with regard to increasing both the numerical aperture and z of hard X-ray FZPs should be addressed. Indeed, even at 7 keV, a z value in excess of 800 nm is typically required to achieve at least 10% efficiency (Kirz, 1974; Yan *et al.*, 2007; Wu *et al.*, 2012). Drawing on the progress made in this area, we herein present a newly developed hard X-ray writer (E = 7.5 keV) based on a FZP and assess the patterning resolution that was achieved by it.

2. Experiment

Experiments were performed at the 9C beamline of the Pohang Light Source in Korea. Fig. 1(*a*) shows a schematic illustration of the experimental setup, in which an X-ray energy of 7.5 keV was selected by a double-crystal Si(111) monochromator. Incident X-rays were then confined to 120 μm × 120 μm by a pair of slits, and were then focused to a nano-spot by a hard X-ray FZP consisting of a gold pattern deposited on a 1 μm-thick SiN membrane through a combination of e-beam lithography and pattern transfer techniques. Details of the fabrication process used for this FZP have been reported elsewhere (Chen *et al.*, 2008, 2011; Wu *et al.*, 2012), and its parameters are summarized in Table 1. Fig. 1(*b*) shows

Table 1
Parameters of the FZP used in this study.

Parameter	Value
Diameter (μm)	110
Total number of zones	689
Outermost zone width (nm)	40
Depth of zones (nm)	947
Focal length at 7.5 keV (mm)	26.7
Theoretical efficiency at 7.5 keV (%)	22.78

a high-magnification scanning electron microscopy (SEM) image near the outermost zones of the FZP. The Δr_n value of this FZP was approximately 40 nm, and the focal length, proportional to the X-ray energy, was 26.7 mm. Note that using such a long focal length in comparison with the several hundred micrometers used with soft X-rays provides substantial experimental advantages when installing lithographic apparatus. A 25 μm-thick Ta pinhole with a diameter of 17 μm was installed 25 mm downstream of the FZP as an order-sorting aperture (OSA) to block all higher-order diffraction signals. No central stop was used. However, the accumulated dose by the direct beam during the patterning process is insignificant in this study because the intensity of the direct beam is very much weaker than that of the focal spot. The X-ray flux at the focus estimated using an X-ray photodiode was 1.2×10^{13} photons mm^{-2} s^{-1}.

In order to evaluate the patterning capability of the X-ray writer, we exposed X-ray nano-spots to a ZEP520A-7 (Zeon Co.) PR which was spin-coated to a thickness of 60 nm onto a single-crystal sapphire(0001) or Si(001) substrate. To achieve the desired pattern, these PR-coated substrates were translated and exposed to the X-ray nano-spots in accordance with a macro coded to control the motion and exposure. Positioning the substrates was controlled using an XYZ stage driven by piezoelectric actuators, while a mechanical shutter (FPS400M, CEDRAT technologies) with a fast response time of 4 ms was used to control the exposure. Note that the hard X-ray writer was operated in air ambient thanks to the high penetration power of hard X-rays, whereas vacuum or He purging is indispensable for soft X-rays. Following patterning in air ambient, exposed samples were immersed in a ZED-N50 (n-amylacetate) developer for 30 s, and then rinsed with isopropyl alcohol for 40 s. This developing process was carried out at 253 K so as to improve the sharpness of the pattern edges, as reported previously (Ocola & Stein, 2006). The developed samples were then dried by air flow. The simple

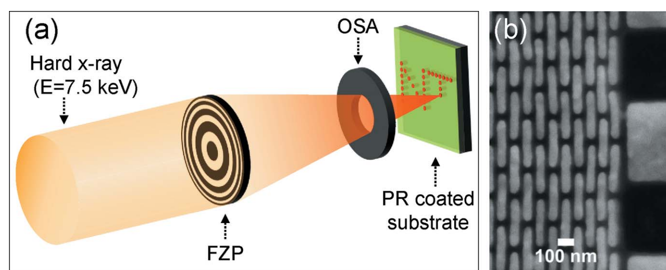

Figure 1
(*a*) Schematic illustration depicting a hard X-ray writer with a FZP. (*b*) High-magnification SEM image of the region near the outermost zone of the FZP. Note that Δr_n is approximately 40 nm.

three-step process as mentioned above was repeated each time. Finally, the morphology and features of thus fabricated patterns were examined by SEM (Jeol, JSM-7500F). The acceleration voltage was 5 kV and the emission current was 20 µA. We note that a thin Pt film was sputtered onto the developed samples prior to SEM measurement. The thickness of the as-deposited Pt film was less than 5 nm.

3. Results and discussion

Fig. 2 shows the SEM images obtained of the letter 'NT' produced by exposing the X-ray nano-spot on a PR-coated sapphire substrate in a controlled array. The exposure was varied within the range 1.4−2.6 s, while the distance between the spots was fixed at 300 nm. A minimum of 1.4 s exposure was necessary to obtain clearly distinguishable spots. In addition, we note that the patterned spots were slightly elliptical in shape due to source demagnification, which is attributed to the undulator property of the synchrotron causing smaller X-ray coherent length in the horizontal direction than in the vertical direction. The focus became relatively large in the horizontal direction. The size of individual spots, determined by averaging the horizontal and vertical size, is displayed in Fig. 3(*a*) as a function of the exposure. As the exposure increased, the size of the spots increased linearly from 36 to 153 nm in the vertical direction, and from 39 to 181 nm in the horizontal direction. The error bars represent the standard deviations for a given set of spots, which was mainly attributed to fluctuations in X-ray dose due to variation in the flux at the focus. The inset of Fig. 2(*a*) shows a high-magnification SEM image that illustrates this deviation in size more clearly.

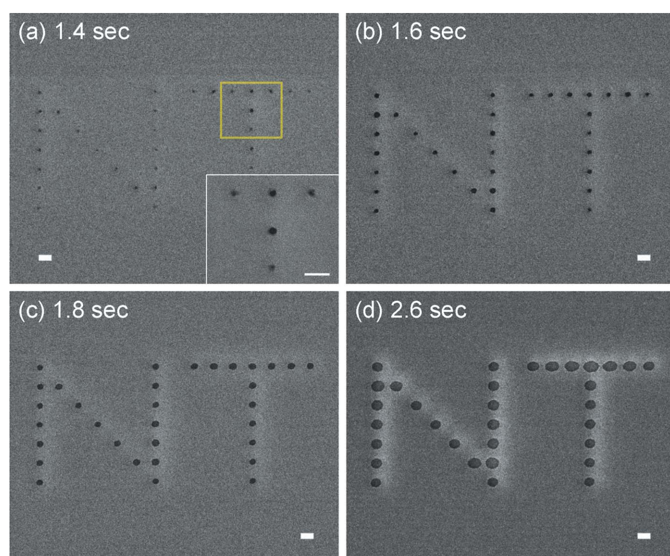

Figure 2
SEM images of the letter 'NT' pattern, an array of spots, produced on PR-coated sapphire substrates with exposure of (*a*) 1.4, (*b*) 1.6, (*c*) 1.8 and (*d*) 2.6 s. The inset of (*a*) shows a high-magnification SEM image taken from the region of interest indicated by the yellow box in (*a*). The scale bars represent 200 nm.

The X-ray exposure sensitivity (R) can be defined simply as $d \sim Rt$, where d is the size of the patterned spots and t is the exposure time, which exhibits a significant correlation with the X-ray induced reaction rate of PR chain-scissoring. The sensitivity in the horizontal and vertical directions was estimated from the slope of the linear fits as being approximately 132 and 100 nm s^{-1}, respectively, which implies that a precise control over exposure time is essential for ensuring pattern uniformity. The sensitivity also depends on the radial spread of electrons. Note that 'electrons' included photoelectrons, Auger electrons and secondary electrons generated from the substrate during X-ray irradiation, as it is well known that PR molecules are broken by these electrons rather than X-ray photons themselves. As the radial spread of these electrons around X-ray nano-spots is inevitable, breaking a patterning resolution below 5 nm could be a huge technological challenge to be overcome in X-ray writers. To examine the effect of these electrons in different substrate types, the patterning process was repeated using the same PR of thickness 60 nm but on a Si(001) substrate. The sensitivity of the PR on the Si(001) substrate is shown in Fig. 3(*b*), which clearly shows that a shorter exposure was required than for the PR on a sapphire substrate to produce a pattern with similar size. The sensitivity of the PR on silicon was 204 nm s^{-1} in the horizontal direction and 166 nm s^{-1} in the vertical direction, which

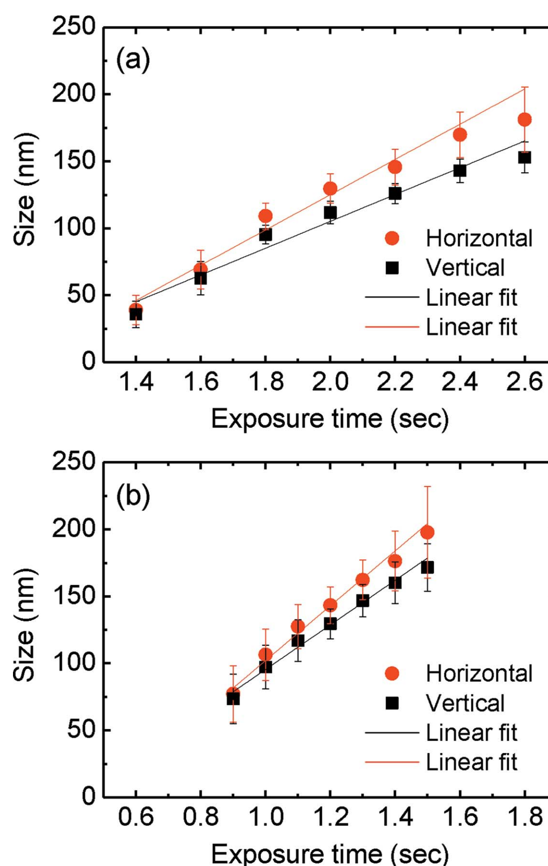

Figure 3
Variation in spot size as a function of the exposure for (*a*) sapphire(0001) and (*b*) Si(001) substrates. The slope of the linear fits represents the X-ray exposure sensitivity. The error bar indicates the standard deviations for a given set of spots.

supports the notion that the radial spread of electrons depends on the substrate material. Specifically, the energy and radial spread of photoelectrons and Auger electrons are sensitive to the substrate material, whereas those of secondary electrons generated by photoelectrons and Auger electrons are much less sensitive to the substrate material (Henke *et al.*, 1977, 1979; Suzuki & Smith, 2007). As the energy of these secondary electrons is typically less than 30 eV, their contribution to the patterning process should be minimal. The energy of the Auger electrons, on the other hand, increases with atomic number. The kinetic energy of the Auger electrons of O, Al and Si atoms is 510, 1396 and 1621 eV, respectively. It can therefore be postulated that the Auger electrons of Si atoms may be the reason for the high sensitivity in Si substrates (Ocola & Cerrina, 1993). In addition, we conjecture that the insulating nature of a sapphire substrate suppresses the migration of electrons.

The proximity effect in e-beam writers is well known to be a result of the radiation spilling over into regions neighboring a targeted position, thereby enlarging the size of the pattern (Chang, 1975). This was observed quite prominently in patterns produced by this X-ray writer. Figs. 4(*a*)–4(*d*) show a series of SEM images taken from a 10 × 10 array of spots on a PR-coated sapphire substrate at different exposure times. In all samples the spots in the outer columns were notably smaller than the others, especially those near the center. This size variation became more significant as the exposure increased, as illustrated in Fig. 4(*e*) which shows the variation in the size of the spots located in the sixth row marked by yellow arrows in Fig. 4(*d*). Note that the vertical (horizontal) size of these spots gradually increases from 111 nm (123 nm) at the edges to 145 nm (174 nm) at the center, which demonstrates the proximity effect on the spot size. The diffuse scattering originated from an intrinsic feature of a focused X-ray beam by a FZP with imperfect zones that produces interference fringes as well as scattered light. The proximity effect was therefore manifested when the spacing between spots is less than 200 nm with prolonged exposure. This caused the spots to come into contact with each other and eliminated the narrow boundaries between them (data not shown). Note that the electron blur near the focus might be a possible source to enhance the proximity effect due to the drastically increased mean free path of the electrons.

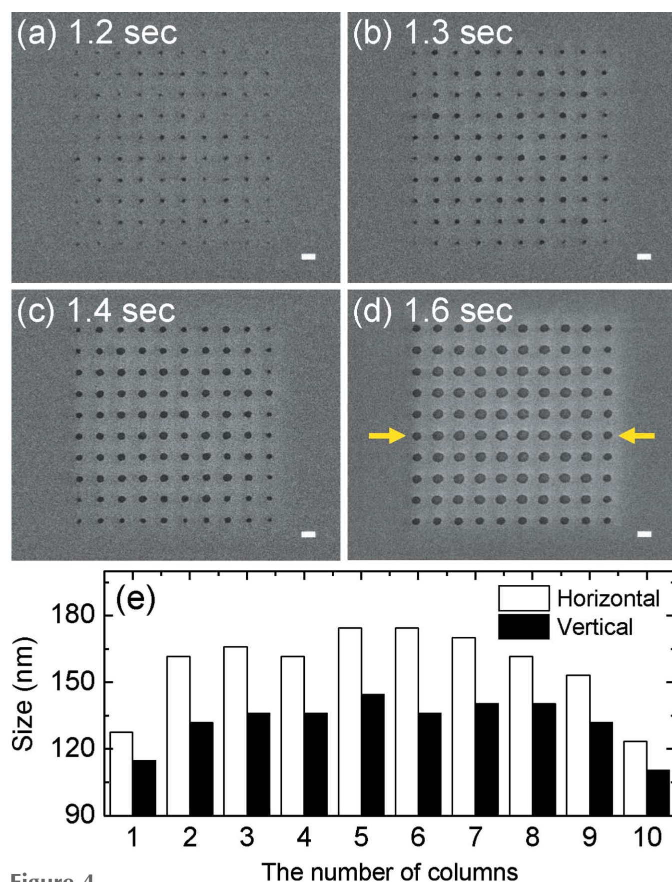

Figure 4
SEM images showing 10 × 10 spot arrays produced with exposure of (*a*) 1.2, (*b*) 1.3, (*c*) 1.4 and (*d*) 1.6 s. Scale bars represent 200 nm. (*e*) Plot of the vertical and horizontal size of spots located within the sixth row, as indicated by the yellow arrows in (*d*).

The resolution of the X-ray writer was examined by patterning numerous individual spots separated by 1 µm, such a large separation being considered sufficient to exclude the proximity effect. A sapphire substrate was used to minimize the contribution of electrons, and the exposure was 1.3 s. An SEM image of the smallest spot produced in this manner with its vertical and horizontal dimensions of 21 and 25 nm, respectively, is illustrated in Fig. 5. This is the best resolution achieved up to now with hard X-rays which is comparable with the best resolution of soft X-ray writers (E = 1 keV) (Leontowich *et al.*, 2013).

4. Conclusions

A hard X-ray writer based on a FZP has been demonstrated to be capable of achieving a resolution of less than 25 nm at E = 7.5 keV. This patterning process was affected strongly by the

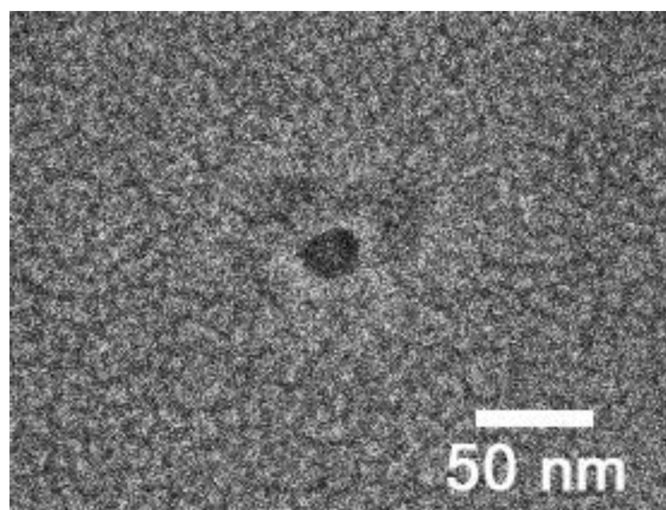

Figure 5
SEM image depicting the patterning resolution of the X-ray writer developed. The spot size was estimated to be 21 and 25 nm in the vertical and horizontal directions, respectively.

underlying substrate type and the radial spread of electrons. No charging effect was observed on the insulating substrate. We, therefore, think that the X-ray writer developed in this work is a promising tool for drawing arbitrary patterns, and could serve as a supplementary technique to existing e-beam writers. Moreover, given that the development of nano-focusing X-ray optics continues to progress toward an ultimate goal of 1 nm, and a 7 nm X-ray spot has been very recently demonstrated (Yamauchi *et al.*, 2011), it is possible that this X-ray writer could ultimately achieve a patterning resolution in the single-digit nanometer range. An alternative approach could be to use a third-order focus, by which the focus size can in principle be reduced by a factor of three. In addition, we recently demonstrated the direct patterning of Ag films with multilayer mask using hard X-rays (Kim *et al.*, 2015), in which periodic patterns with a line width as small as 21 nm were fabricated. Such a direct patterning technique on metal thin films without the typical photo-resist process should be a possible application of X-ray writers. There are, however, still various challenges that should be addressed to suppress the proximity effect and to reduce strong electrons, as well as identifying PR materials suitable for hard X-ray writers.

Acknowledgements

We would like to acknowledge Chan Kim and Yoonhee Kim for their support in preparation of the experimental setup. This research was supported by the National Research Foundation of Korea (NRF) grant funded by the Korean government (MSIP) through NCRC (No. 2008-0062606, NCRC-CELA), and general research program (2010-0023604). We also acknowledge the GSG Project through a grant provided by GIST in 2014 and the support by Institute for Basic Science (IBS). The work was also partially supported by PAL, XFEL project, Korea. This work (grant No. C0221415) was also partially supported by Business for Academic–Industrial Cooperative Establishments funded Korea Small and Medium Business Administration in 2014.

References

Bergemann, C., Keymeulen, H. & van der Veen, J. F. (2003). *Phys. Rev. Lett.* **91**, 204801.
Caster, A. G., Kowarik, S., Schwartzberg, A. M., Leone, S. R., Tivanski, A. & Gilles, M. K. (2010). *J. Vac. Sci. Technol. B*, **28**, 1304–1313.
Chang, T. H. P. (1975). *J. Vac Sci. Technol.* **12**, 1271–1275.
Chao, W., Fischer, P., Tyliszczak, T., Rekawa, S., Anderson, E. & Naulleau, P. (2012). *Opt. Express*, **20**, 9777–9783.
Chen, T.-Y., Chen, Y.-T., Wang, C.-L., Kempson, I. M., Lee, W.-K., Chu, Y. S., Hwu, Y. & Margaritondo, G. (2011). *Opt. Express*, **19**, 19919–19924.
Chen, Y., Lo, T., Chu, Y., Yi, J., Liu, C., Wang, J., Wang, C., Chiu, C., Hua, T., Hwu, Y., Shen, Q., Yin, G. C., Liang, K. S., Lin, H. M., Je, J. H. & Margaritondo, G. (2008). *Nanotechnology*, **19**, 395302.
Chou, S., Krauss, P., Zhang, W., Guo, L. & Zhuang, L. (1997). *J. Vac. Sci. Technol. B*, **15**, 2897–2904.
Gan, Z., Cao, Y., Evans, R. A. & Gu, M. (2013). *Nat. Commun.* **4**, 2061.
Henke, B. L., Liesegang, J. & Smith, S. D. (1979). *Phys. Rev. B*, **19**, 3004–3021.
Henke, B. L., Smith, J. & Attwood, D. T. (1977). *J. Appl. Phys.* **48**, 1852–1866.
Huang, X., Yan, H., Nazaretski, E., Conley, R., Bouet, N., Zhou, J., Lauer, K., Li, L., Eom, D., Legnini, D., Harder, R., Robinson, I. K. & Chu, Y. S. (2013). *Sci. Rep.* **3**, 3562.
Kang, H., Maser, J., Stephenson, G., Liu, C., Conley, R., Macrander, A. & Vogt, S. (2006). *Phys. Rev. Lett.* **96**, 127401.
Keskinbora, K., Robisch, A.-L., Mayer, M., Sanli, U. T., Grévent, C., Wolter, C., Weigand, M., Szeghalmi, A., Knez, M., Salditt, T. & Schütz, G. (2014). *Opt. Express*, **22**, 18440–18453.
Kim, J. M., Lee, S. Y., Kang, H. C. & Noh, D. Y. (2015). *J. Synchrotron Rad.* **22**, 156–160.
Kirz, J. (1974). *J. Opt. Soc. Am.* **64**, 301–309.
Leontowich, A. F. G. & Hitchcock, A. P. (2011). *Appl. Phys. A*, **103**, 1–11.
Leontowich, A., Hitchcock, A., Watts, B. & Raabe, J. (2013). *Microelectron. Eng.* **108**, 5–7.
Macintyre, D. S. & Thoms, S. (2011). *J. Vac. Sci. Technol. B*, **29**, 06F307.
Mimura, H., Handa, S., Kimura, T., Yumoto, H., Yamakawa, D., Yokoyama, H., Matsuyama, S., Inagaki, K., Yamamura, K., Sano, Y., Tamasaku, K., Nishino, Y., Yabashi, M., Ishikawa, T. & Yamauchi, K. (2009). *Nat. Phys.* **6**, 122–125.
Ocola, L. & Cerrina, F. (1993). *J. Vac. Sci. Technol. B*, **11**, 2839–2844.
Ocola, L. E. & Stein, A. (2006). *J. Vac. Sci. Technol. B*, **24**, 3061–3065.
Satyalakshmi, K., Olkhovets, A., Metzler, M., Harnett, C., Tanenbaum, D. & Craighead, H. (2000). *J. Vac. Sci. Technol. B*, **18**, 3122–3125.
Schroer, C., Kurapova, O., Patommel, J., Boye, P., Feldkamp, J., Lengeler, B., Burghammer, M., Riekel, C., Vincze, L., van der Hart, A. & Küchler, M. (2005). *Appl. Phys. Lett.* **87**, 124103.
Schroer, C. G. & Lengeler, B. (2005). *Phys. Rev. Lett.* **94**, 054802.
Suzuki, K. & Smith, B. (2007). *Microlithography: Science and Technology.* Boca Raton: CRC Press.
Winston, D., Manfrinato, V. R., Nicaise, S. M., Cheong, L. L., Duan, H., Ferranti, D., Marshman, J., McVey, S., Stern, L., Notte, J. & Berggren, K. K. (2011). *Nano Lett.* **11**, 4343–4347.
Wu, S., Hwu, Y. & Margaritondo, G. (2012). *Materials (Basel)*, **5**, 1752–1773.
Yamauchi, K., Mimura, H., Kimura, T., Yumoto, H., Handa, S., Matsuyama, S., Arima, K., Sano, Y., Yamamura, K., Inagaki, K., Nakamori, H., Kim, J., Tamasaku, K., Nishino, Y., Yabashi, M. & Ishikawa, T. (2011). *J. Phys. Condens. Matter*, **23**, 394206.
Yan, H., Maser, J., Macrander, A., Shen, Q., Vogt, S., Stephenson, G. B. & Kang, H. C. (2007). *Phys. Rev. B*, **76**, 115438.